OPEN ACCESS Freely available online

PLoS one

Ligand Depletion *in vivo* Modulates the Dynamic Range and Cooperativity of Signal Transduction

Stuart J. Edelstein, Melanie I. Stefan, Nicolas Le Novère*

European Bioinformatics Institute, Hinxton, United Kingdom

Abstract

Biological signal transduction commonly involves cooperative interactions in the binding of ligands to their receptors. In many cases, ligand concentrations *in vivo* are close to the value of the dissociation constant of their receptors, resulting in the phenomenon of ligand depletion. Using examples based on rotational bias of bacterial flagellar motors and calcium binding to mammalian calmodulin, we show that ligand depletion diminishes cooperativity and broadens the dynamic range of sensitivity to the signaling ligand. As a result, the same signal transducer responds to different ranges of signal with various degrees of cooperativity according to its effective cellular concentration. Hence, results from *in vitro* dose-response analyses cannot be applied directly to understand signaling *in vivo*. Moreover, the receptor concentration is revealed to be a key element in controlling signal transduction and we propose that its modulation constitutes a new way of controlling sensitivity to signals. In addition, through an analysis of the allosteric enzyme aspartate transcarbamylase, we demonstrate that the classical Hill coefficient is not appropriate for characterizing the change in conformational state upon ligand binding to an oligomeric protein (equivalent to a dose-response curve), because it ignores the cooperativity of the conformational change for the corresponding equivalent monomers, which are generally characterized by a Hill coefficient $\ll 1$. Therefore, we propose a new index of cooperativity based on the comparison of the properties of oligomers and their equivalent monomers.

Citation: Edelstein SJ, Stefan MI, Le Novère N (2010) Ligand Depletion *in vivo* Modulates the Dynamic Range and Cooperativity of Signal Transduction. PLoS ONE 5(1): e8449. doi:10.1371/journal.pone.0008449

Editor: Vladimir Brezina, Mount Sinai School of Medicine, United States of America

Received October 7, 2009; **Accepted** November 27, 2009; **Published** January 5, 2010

Funding: S.E. acknowledges support from the Wellcome Trust. The funders had no role in study design, data collection and analysis, decision to publish, or preparation of the manuscript.

Competing Interests: The authors have declared that no competing interests exist.

* E-mail: lenov@ebi.ac.uk

Introduction

Dose-response is one of the most common experimental approaches used by biologists to monitor the properties of signaling molecules. The power of this approach arises from the fact that the change in any quantifiable physiological response can be measured as a function of the chemical stimulus responsible. In some cases, the resulting curve is sigmoidal, which generally implies cooperative interactions between the binding sites for the ligand that initiates the response (but other explanations are possible — see below). In general, cooperativity (or ultrasensitivity) arises for numerous biological processes regulated by protein-protein or protein-ligand interactions involving multi-site proteins that transduce signals via conformational isomerization [1–3].

Cooperativity has been represented for numerous oligomeric protein systems by the allosteric model of concerted transitions [1]. The model is based on spontaneous transitions between two conformational states, designated T (for "tense") and R (for "relaxed"). The governing principle of the model is that in the absence of any bound ligands, the T conformation is energetically favored over the R conformation. However, because the R conformation has a higher affinity than the T state for a ligand specific for the protein under consideration, the presence of ligand pulls the $T-R$ equilibrium towards the R state. Under these conditions, a clear distinction can be made between two mathematical functions that describe the behavior of protein-ligand interactions as a function of ligand concentration: 1) the binding function, $\bar{Y}$, defined as the fractional occupancy of the ligand binding sites of the protein, taking into account both the T and R states; and 2) the state function, $\bar{R}$, defined as the fraction of molecules in the R state. The state function $\bar{R}$ corresponds closely to what is measured by dose-response analysis for an allosteric "receptor" protein. The definitions of $\bar{Y}$, $\bar{R}$, and various related parameters are summarized in Table 1.

From its initial application to the sigmoidal oxygen-binding curve of hemoglobin, cooperativity has been conveniently characterized by the Hill coefficient, n_H [4,5]. The value of n_H is obtained as the slope of the Hill plot: the logarithm of the ratio of occupied to unoccupied binding sites on the ordinate is given as a function of the logarithm of the ligand concentration on the abscissa. The value of n_H provides an empirical index of cooperativity: its upper limit is the number of interacting sites and its value is directly related to non-cooperative systems, since for a monomeric protein with a single site, $n_H = 1$. The Hill coefficient is widely used, including for dose-response curves, but care must be taken in interpreting its value [6–8], since kinetic effects can alter apparent cooperativity [9] and even a monomeric enzyme can display cooperative behavior, i.e. $n_H > 1.0$ [10,11].

Cooperativity can also be generated by relatively simple networks [12], for example through competition between two sets of phosphorylation sites [13], as well as sequestration effects involving an inactive complex [14] or more complex signal transduction cascades [15]. The interpretation of values of $n_H < 1$, which can be a sign of negative cooperativity [16], also requires careful attention,

Table 1. Summary of terms for cooperativity and ligand depletion.

Term	Description	Equation
α	The concentration of ligand normalized to the affinity of the R state	3
α_{50}	The value of α corresponding to $\bar{R}=0.5$	16
α_{total}	The value of α comprising both free and bound ligand	9
c	The ratio of ligand dissociation constants for the R and T states	2
C_s	The molar concentration of ligand binding sites	9
L	The allosteric constant governing the intrinsic $T-R$ equilibrium	1
n_H	The Hill coefficient, defined by slope of loglog plot	18
n_{50}	The Hill coefficient at α_{50}	—
λ	The allosteric constant governing the intrinsic equivalent monomers T^*-R^* equilibrium	10
v	Cooperativity of the state function for an oligomer relative to the equivalent monomer	15
v_{max}	The maximal value of v, which occurs at α_{50}	16
Ω	The ligand stabilization factor for T over R	6
R	The "relaxed" (high affinity) conformational state	1
$\bar{R}$	Fraction of total molecules (T and R) in the R state as a function of α	5
$\bar{R}'$	$\bar{R}$ as a function of the total concentration ligand (free and bound)	9
$\bar{R}^*$	The fraction of equivalent monomers (T^* and R^*) in the R^* state	12
T	The "tense" (low affinity) conformational state	1
X	Any ligand	3
$\bar{Y}$	Fraction of all binding sites (T and R) occupied by ligand	4
$\bar{Y}^*$	Fraction of equivalent monomer binding sites occupied by ligand	17
$\bar{Y}'$	$\bar{Y}$ as a function of the total concentration of ligand (free and bound)	—

doi:10.1371/journal.pone.0008449.t001

since even for hemoglobin, binding curves with $n_H<1$ can be generated in the presence of non-stoichiometric concentrations of the positive effector, 2,3-diphosphoglycerate [17].

In addition to cooperativity, the non-linear properties of ultrasensitive systems define a dynamic range of signal intensities for which the responses vary. The greater the degree of cooperativity for a system with respect to signal changes, the narrower the dynamic range over which the response varies. For highly cooperative systems, such as bacterial chemotaxis, elaborate mechanisms have evolved in order to extent the dynamic range of response to changes in the concentrations of attractants or repellants [18,19].

For all signal transduction systems considered, a predominant effect under physiological conditions is ligand depletion. When the concentrations of receptors are close to the dissociation constant for the relevant ligand, the free concentration of the ligand falls significantly below the total concentration of ligand, which in fact constitutes the actual input signal. This effect can be particularly important under *in vivo* conditions, for which most protein concentrations and dissociation constants are within the nano- to micro-molar range. The general principle of ligand depletion has been widely recognized [20–22] and various aspects have been considered for biological networks [14,15,23]. Here we focus on the consequences of ligand depletion with respect to cooperativity and dynamic range, as visualized for two extreme systems. First, we examine the highly cooperative flagellar motor system [24,25]. Second, we turn to the minimally cooperative, but ubiquitous example of calmodulin [26,27] in order to explore the consequences of ligand depletion under diverse conditions that apply in distinct regions of the brain and other organs. Finally, after illustrating why the Hill coefficient is not appropriate for measuring cooperativity of signal transduction, we define a new index of cooperativity, v, as illustrated with the classical example of the allosteric enzyme aspartate transcarbamylase [28,29]. We show that v, based on the introduction of an "equivalent monomer" concept, is a reliable measure of cooperativity for dose-response type curves under all conditions.

Results

Ligand Depletion and Dynamic Range in the Flagellar Motor System

We illustrate the importance of considering ligand depletion with the highly cooperative *E. coli* flagellar motor system [30], which controls the direction of flagellar rotation in response to the concentration of phosphorylated CheY [31]. The rotational bias of individual motors as a function of CheY-P has been measured using tethered single cells and GFP-CheY [30]. The motor bias reflects a change of rotation from counter-clockwise to clockwise and therefore a change of fractional activation (or state function, $\bar{R}$), which is influenced by the interaction of CheY-P with the 34 units of FliM comprising the motor ring [32]. The data show a high degree of cooperativity, with Hill coefficients of up to 10 reported [30]. In contrast, the fractional occupancy, measured using FRET between CheY and FliM appears to be much less cooperative [31].

For dose-response measurements it is reasonable to assume equivalence to within experimental errors of the concentrations of the free and total ligand only if the protein to which the ligand is bound is present at sufficiently low concentration compared to the dissociation constant. However, for the measurements of the flagella motor system, free and total ligand were determined directly and were found to be far from equivalent [31]. The free

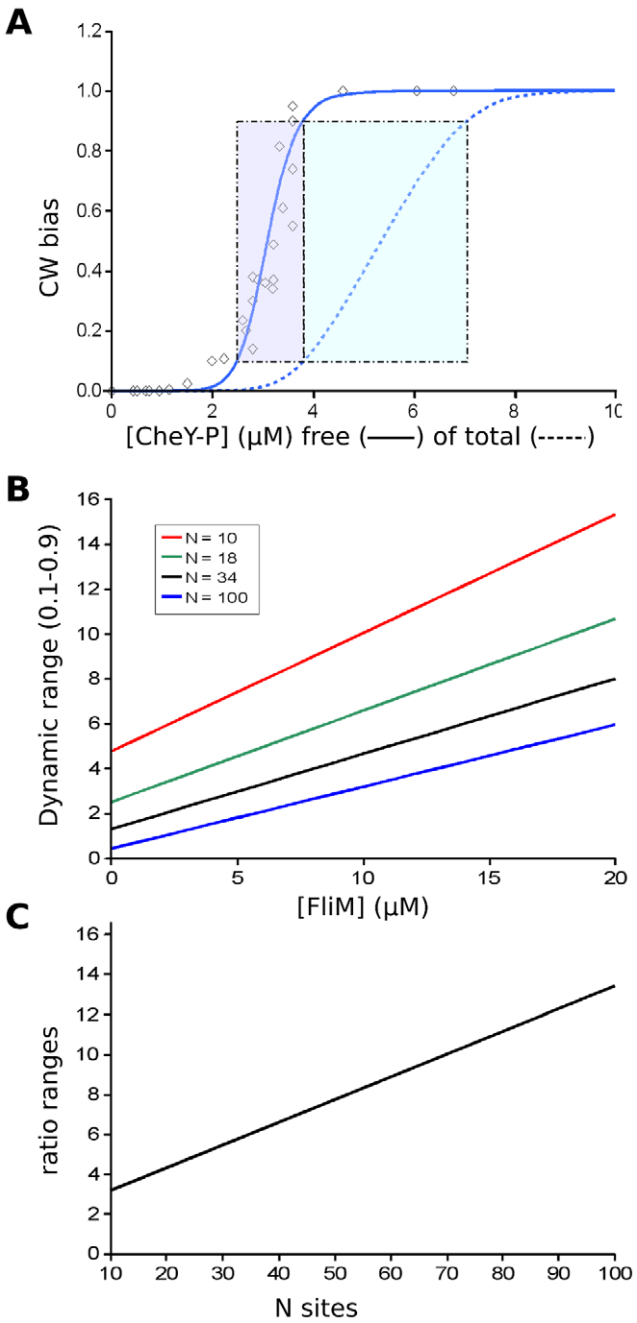

Figure 1. Flagellar motor model. (A) Curves for $\bar{R}$ as a function of the concentration of free CheY-P (no ligand depletion: solid blue line) and curves for $\bar{R}'$ as a function of total CheY-P (with ligand depletion: dashed blue line), with $\bar{R}$ and $\bar{R}'$ expressed in terms of CW bias, the measured parameter of the flagellar motor corresponding to the fraction of time undergoing clockwise rotation. The dynamic range, defined as the ligand concentration range between values of $\bar{R}$ or $\bar{R}'$ of 0.1 and 0.9, is represented by the shaded rectangles for the curves with and without ligand depletion. The open diamond points correspond to the measurements reported by Cluzel et al. [30]. (B) Variations in the dynamic range due to ligand depletion as a function of the concentration of FliM for values of N (the number of sites) = 10, 18, 34, and 100. For each value of N, the curve for $\bar{R}$ is computed based on an L value set by $L=\lambda^N$ (see Materials and Methods, Eqn 11), where λ is fixed by the value used for $N=34$, i.e. $\lambda=(4\times10^7)^{(1/34)}$. (C) The ratio of the dynamic range for $[\mathrm{FliM}]=20\mu\mathrm{M}$ to the dynamic range for $[\mathrm{FliM}]=0$ as a function of N, the number of sites and calculated as in (B). Parameter values used for the curves in (A): $L=4\times10^7$, $K_T=10^{-5}$ M, $K_R=2\times10^{-6}$ M, and $N=34$, with a concentration of $\mathrm{FliM}=5.8\times10^{-6}$ M. Calculation of ligand depletion effects as described in Eqn 9 of the Material and Methods section.
doi:10.1371/journal.pone.0008449.g001

concentration is significantly reduced compared to the total concentration, due to binding to FliM, as well as to CheA and CheZ [33]. In order to characterize this effect, we define $\bar{R}'$, the response as a function of the total ligand concentration, which is distinct from $\bar{R}$, the response as a function of the free ligand concentration (see Table 1).

When ligand-depletion effects are taken into account, the curve for $\bar{R}'$ is displaced far to the right of the curve for $\bar{R}$ (Figure 1A). In addition, $\bar{R}'$ is significantly less steep than $\bar{R}$. Moreover, the effect of ligand depletion on response curves is exhibited by all cooperative frameworks based on thermal equilibria, not only strictly concerted-models, such as proposed by Duke et al [34]. Therefore, ligand depletion results in an increase in the dynamic range of signal concentrations sensed by the system, as measured for instance by the differences in total concentration of CheY-P corresponding to $\bar{R}'$ values between 0.1 and 0.9, which increase from 3.8μM to 7.1μM for a full change of response in this range. In comparison, the results presented using $\bar{R}$ without taking into account ligand depletion could contribute to an underestimation of the dynamic range, since equivalent response changes would be achieved by increase from 2.5μM to 3.8μM. With variations in the concentration of FliM, the dynamic range increases linearly (Figure 1B). More generally for multisite receptors, the dynamic range varies with the number of subunits, as observed for the family of curves in Figure 1B and 1C. Ligand depletion may also account for the discrepancies observed between the results reported by Cluzel et al [30] and other studies [35,36] showing a much lower apparent cooperativity.

The Effect of Ligand Depletion on the Response Characteristics of Calmodulin

In contrast to the behavior of a system of high cooperativity as described above, we examined the properties of calmodulin, a key molecule of calcium signaling with relatively low cooperativity [37], for which an analysis based on the MWC model has recently been presented [38]. The protein exists as a small monomer (148 residues), with four distinct calcium binding sites, each characterized by specific dissociation constants for calcium that vary between the low-affinity and high-affinity states [38]. Although the reference ligand binding properties that we used for our analysis are free of ligand-depletion effects [39], we have transformed the data to simulate conditions of ligand depletion, with points that fit the curve for $\bar{Y}'$ (the fractional occupancy as a function of the total calcium concentration) for calmodulin at 40μM (Figure 2A). In addition, we have calculated a series of response curves presented in Figure 2A for the activation of calmodulin by calcium both under conditions with no ligand depletion ($\bar{R}$), as well as under condition with ligand depletion ($\bar{R}'$) corresponding to various concentration of calmodulin found in vivo [40]. The differences between $\bar{R}$ and $\bar{R}'$ are very clear, including a progressive broadening of the dynamic range, with markedly diminished cooperativity as the concentration of calmodulin increases. The corresponding decreases in cooperativity as a function of calmodulin concentration are presented in Figure 2B, showing a dramatic fall off with concentration from the initial value ≈ 2 under conditions where Ca^{2+} is in large excess, to cooperativity values for the highest concentrations approaching zero.

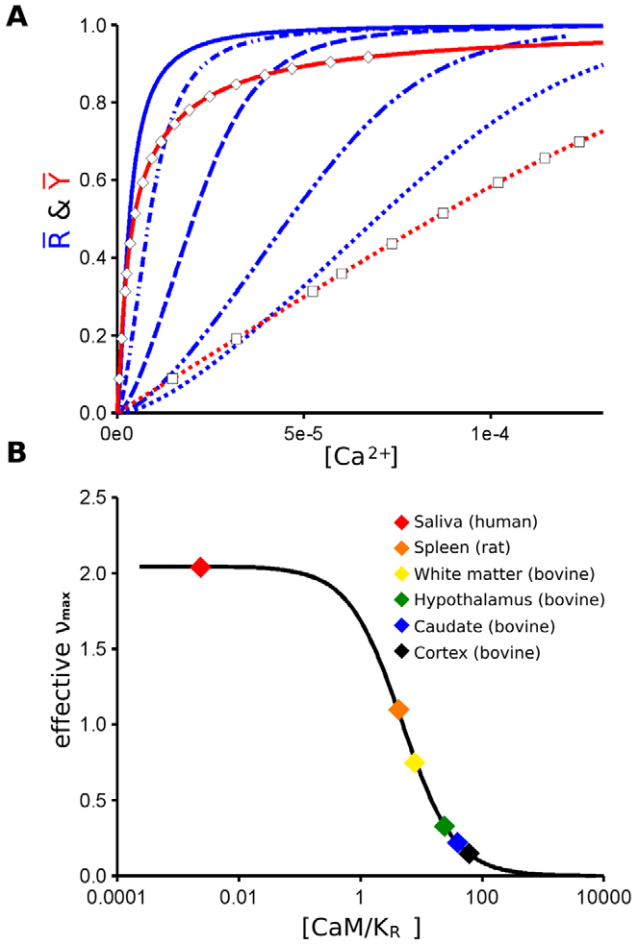

Figure 2. Ligand depletion for calmodulin. (A) Curves for $\bar{R}'$ (blue) and $\bar{Y}'$ (red) as a function of the calcium concentration. (B) Values of effective cooperativity v_{max} as a function of calmodulin (CaM) concentration/K_R, where K_R is the affinity of the R state for calcium. For the curves with solid lines in (A), $[\mathrm{CaM}]=10^{-7}$ M and no ligand depletion occurs; the dashed curves for $\bar{R}'$ present conditions of ligand depletion based on the bovine brain calmodulin concentrations of white matter: 3.3μM (- - - . - - -); hypothalamus: 10.4μM (- - -); caudate nucleus: 16.8μM (. . - . .); and cortex: 25.9μM (. . . .), as reported by Kakiuchi et al. [40] or for $\bar{Y}'$ with the concentration of 40μM used in the measurements by Porumb [39], with data points shown as open squares. Although the calmodulin concentration of 4×10^{-5} M [39] was close to the in vivo concentration of 5×10^{-5} M in dendritic spines [60], the data were obtained by flow dialysis, which relates binding to the free calcium concentration, such that ligand depletion effects can be ignored, but we have transformed the data to simulate conditions of ligand depletion, with experimental points that closely follow the curve for $\bar{Y}'$, the fractional occupancy as a function of the total calcium concentration. The same calcium concentrations in (A) are used for the calculations in (B), with the addition of a value for saliva and rat spleen [40,61]. Other parameter values as published previously [38] obtained using data from several sources. The curves under conditions of ligand depletion in (A) are calculated as described in the legend to Figure 1. Cooperativity in B is expressed in relation to the effective value of the index v_{max} (Table 1), which decreases as a function of the total concentration of CaM.
doi:10.1371/journal.pone.0008449.g002

Limitations of the Hill Coefficient for Dose-Response Measurements and Introduction of a New Index Applied to Aspartate Transcarbamylase

Since cooperativity of binding is generally evaluated by the Hill coefficient, n_H, it is not surprising that the Hill coefficient has also been used to characterize many cooperative biological processes, including the fractional activation of signaling receptors and other proteins. However, as we shall demonstrate here, for conformational isomerization of a multi-site protein, n_H is not a reliable measure of cooperativity. In contrast to the cooperativity of $\bar{Y}$, which varies with the energy difference of the two conformational states, as specified by the conformational isomerization constant, L, the value of n_H for $\bar{R}$ is independent of the value of L [41], as shown in Figure 3. When conditions of low, intermediate, and high affinity are examined for a hypothetical hexamer (Figure 3, left panels), the corresponding n_H curves for cooperativity (Figure 3, middle panels) change appropriately for $\bar{Y}$, but are identical for $\bar{R}$ in the three cases. As a result, when cooperativity is examined as a function of $\bar{Y}$ (Figure 3, right panels), the point of maximal cooperativity moves to the right for n_H of $\bar{Y}$ as affinity decreases, but the maximum value n_H for $\bar{R}$ displays the opposite pattern.

Since n_H does not vary with the energetic difference of the two states, the shape of the curves for $\bar{R}$ when expressed as Hill plots are invariant for different L values, as shown in Figure 4. In contrast to the Hill plots of $\bar{Y}$, for which the shape changes as a function of L values, the curves for $\bar{R}$ change only vertical position, not shape. Since cooperativity is generally measured around 50% response, correct results are obtained for $\bar{Y}$, but the apparent cooperativity of $\bar{R}$ at 50%, i.e. $\log[\bar{R}/(1-\bar{R})]=0$ for a Hill plot, depends on the vertical position of the curve for $\log[\bar{R}/(1-\bar{R})]$ and is only a valid estimate of cooperativity for $L\approx c^{-n/2}$ (Figure 4, green curve). The differences in shape between the curves for $\log[\bar{Y}/(1-\bar{Y})]$ and $\log[\bar{R}/(1-\bar{R})]$ also explain why the cooperativity curves in Figure 3 (middle panels) tend towards $n_H=1$ at the extremes for $\bar{Y}$, but towards $n_H=0$ at the extremes for $\bar{R}$. Values of $n_H<1$ are commonly considered to be characteristic of negative cooperativity rather than the absence of cooperativity, but the properties of $\bar{R}$ curves represent a special case for which the conventional reasoning does not apply. Overall, the analyses presented in Figures 3 and 4 make clear that as a general parameter to characterize $\bar{R}$ under any conditions, the Hill coefficient is not a reliable measure of cooperativity.

In order to overcome the limitations of the Hill coefficient applied to $\bar{R}$, we reexamined how cooperativity is computed for conformational isomerization using data for the allosteric enzyme aspartate transcarbamylase (ATCase), one of the original examples of allosteric phenomenon [42]. Following the formulation of the two-state MWC model [1], it was recognized that under many conditions, $\bar{Y}$ and $\bar{R}$ as a function of ligand concentration would not overlap [43]. In a classic study of ATCase, the direct binding of succinate ($\bar{Y}$) was compared to the succinate-dependent conformational change ($\bar{R}$) as measured by sedimentation or reactivity of protein sulfydryl groups [44,45]. ATCase was initially characterized as a tetramer, but later studies revealed a hexamer [46,47] and subsequent structural studies have thoroughly characterized the two hexameric conformational states, T and R, and their concerted interconversion [48,49]. Using the parameters of the MWC model established for $\bar{Y}$ and $\bar{R}$ data on the basis of four sites, the theoretical curves were recalculated with six sites, as presented in Figure 5. Under the experimental conditions employed, the curve for $\bar{R}$ is substantially to the left of the curve for $\bar{Y}$, which constituted strong evidence a conformational equilibrium pre-existing to ligand binding [45]. When the Hill coefficients are determined at 50% for both the $\bar{Y}$ and $\bar{R}$ curves, the value of $n_H=1.24$ for $\bar{Y}$ is a reliable measure of the cooperativity, but the value of $n_H=1.12$ for $\bar{R}$ dramatically underestimates the intrinsic cooperativity, as we now demonstrate.

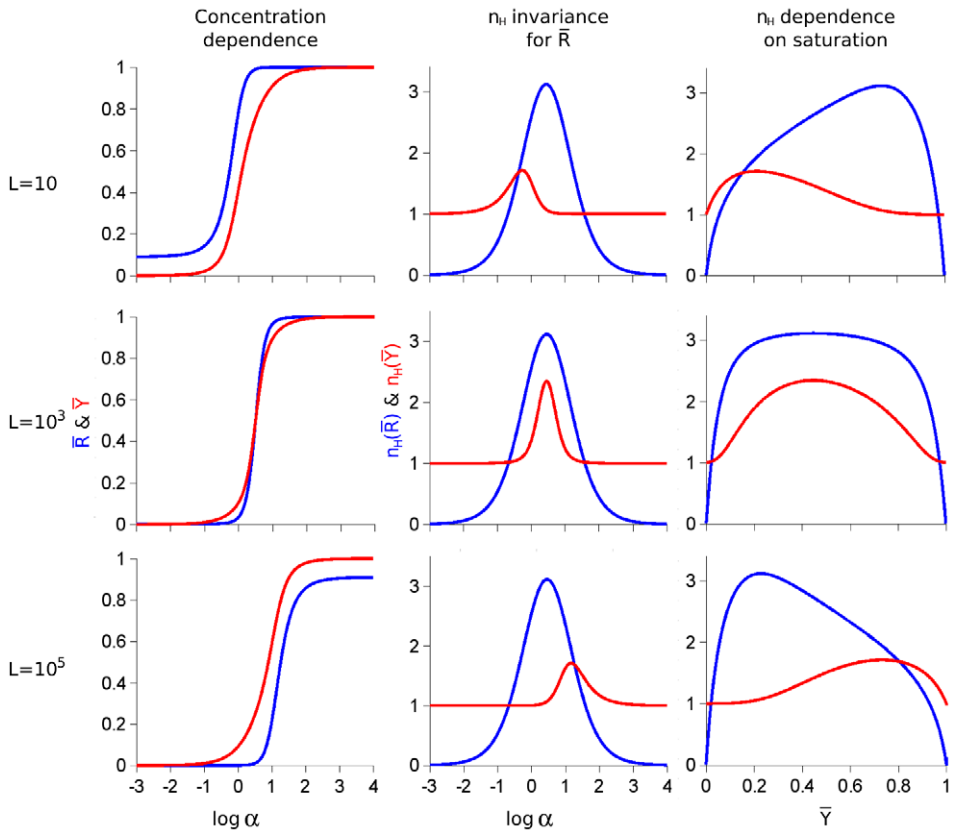

Figure 3. Dependence of $\bar{R}$ and $\bar{Y}$ and their respective Hill coefficients (n_H) on the value of L. Three values of L are illustrated, low L ($L=10$; top three panels); intermediate L ($L=1000$; middle three panels — this value corresponds to the maximal cooperativity for the value of c used: $L=c^{-N/2}$, where N is the number of subunits or binding sites: $N=6$); and high L ($L=100000$; lower three panels). For each line of panels, the curves for $\bar{R}$ (blue) and $\bar{Y}$ (red) are in the left panels, while the Hill coefficient (n_H) is presented as a function of α (middle panels) or of $\bar{Y}$ (right panels), in both cases for $\bar{R}$ (blue) and $\bar{Y}$ (red). The three panels of the central column illustrate that n_H is invariant for $\bar{R}$ as function of L. Therefore, as function of $\bar{Y}$ (three panels of the right column), the maximal value of n_H for R is at a high value of $\bar{Y}$ for low L (upper right panel) and at a low value of $\bar{Y}$ for high L (lower right panel).
doi:10.1371/journal.pone.0008449.g003

In order to establish the correct intrinsic cooperativity of an oligomeric protein undergoing conformational isomerization, a reference state is required that corresponds to a hypothetical equivalent monomer, characterized by same intrinsic affinities for ligand of the R and T states. A conformational transition of the equivalent monomer as a function of the binding of its ligand can be defined and is represented here by $\bar{R}^*$, along with the binding to the equivalent monomer represented by $\bar{Y}^*$. For an equivalent monomer, the energy difference between the T and R states is postulated to be $1/N$ of the energy for the oligomer, since the energy difference for the oligomer is spread equally over the N subunits. Therefore, we define λ, a conformational isomerization parameter for the equivalent monomer, where $\lambda=\sqrt[N]{L}$ (see also Materials and Methods, Eqn 11). When the curves for $\bar{R}$ and $\bar{R}^*$ are compared as in Figure 5A, they cross at the value of 0.5 (which is true for all symmetrical MWC-type systems), but the curve for the equivalent monomer is clearly much more shallow.

With respect to ligand binding, the curves for $\bar{Y}$ and $\bar{Y}^*$ in Figure 5A differ only slightly and are characterized by Hill coefficients of $n_H=1.241$ and $n_H=1.000$, respectively. In contrast, the $\bar{R}^*$ curve, with a Hill coefficient of $n_H=0.187$ is much less cooperative than the curve for $\bar{R}$, with $n_H=1.12$, exactly 6-fold higher than the value for $\bar{R}^*$. In general, under virtually all conditions $\bar{R}^*$ is characterized by a value of the Hill coefficient, $n_H<1$ (see Figure 6).

In order to overcome the insensitivity of n_H for $\bar{R}$ to L (Figure 3) and to rely on an appropriate reference state corresponding to the equivalent monomer, we propose replacing the Hill coefficient for dose-response type behavior by a new cooperativity index, ν (Greek letter nu), based on the ratio of the derivatives of the functions for $\bar{R}$ and $\bar{R}^*$. The function ν therefore corresponds to the ratio of the slopes exhibited by the responses of the cooperative protein and its equivalent non-cooperative monomer. When the new derivative functions are calculated, for $\bar{R}=\bar{R}^*=0.5$ for the ATCase data in Figure 5, the values of the derivatives are 0.710 and 0.118, respectively, with a ratio of 6.0. The new cooperativity index ν can also be computed directly from the definition of $\bar{R}$ and $\bar{R}^*$ (see Material and Methods, Eqn 15). For ATCase, direct calculation also yields $\nu_{max}=6.0$.

The revised analysis of ATCase illustrates that the intrinsic cooperativity at $\bar{R}=0.5$ is always maximal, i.e. equal to the number of binding sites (N), when compared to the equivalent monomer reference state for symmetrical oligomeric proteins. In other words, for a multi-site protein that undergoes a concerted conformational transition, as defined by the MWC model [1], the maximal cooperativity is always equivalent to the number of ligand-binding sites present and may be grossly underestimated on the basis of the Hill coefficient. This property reflects the absolute linkage, or infinite junctional energy, between binding sites in the MWC framework [34]. When data for the flagellar motor is re-examined in this context,

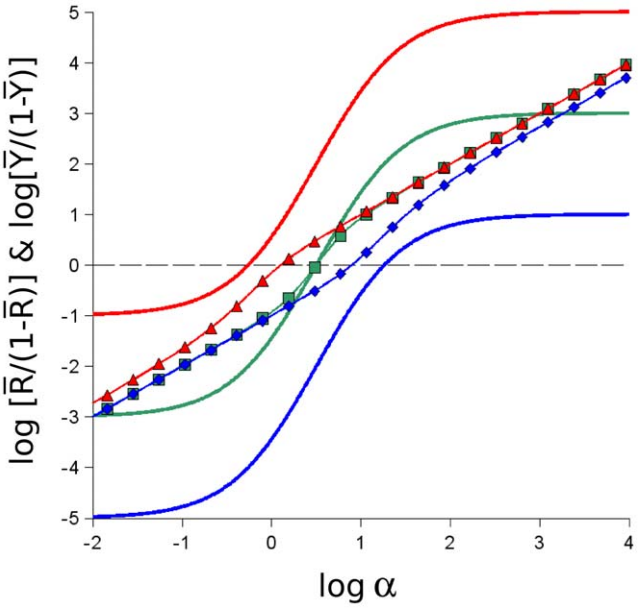

Figure 4. Hill plots for $\bar{R}$ and $\bar{Y}$. The data of Figure 3 (left column) are presented converted to the Hill plot, with the ordinate in the form of $\log[\bar{R}/(1-\bar{R})]$ or $\log[\bar{Y}/(1-\bar{Y})]$. For the three values of L (10, red curves; 1000, green curves; or 100000, blue curves) the data for $\bar{R}$ (solid lines) appear as parallel curves displaced vertically as a function of L. In contrast, the data for $\bar{Y}$ (triangles for $L=10$, open squares for $L=1000$, diamonds for $L=100000$) vary with the inflection points displaced progressively to the right with increasing magnitude of L.
doi:10.1371/journal.pone.0008449.g004

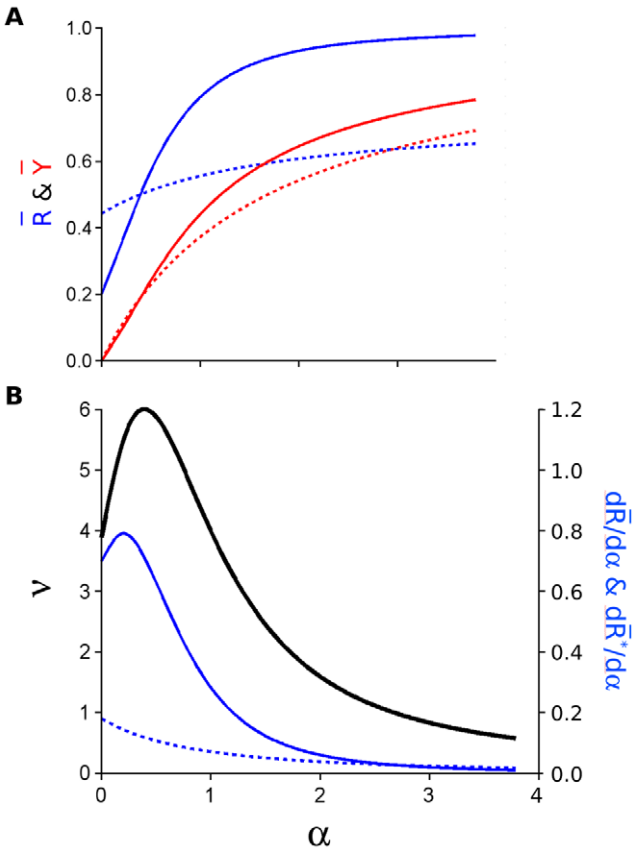

Figure 5. New measure of cooperativity for aspartate transcarbamylase based on an equivalent monomer. (A) Curves for $\bar{R}$ and $\bar{R}^*$ (in blue) and $\bar{Y}$ and $\bar{Y}^*$ (in red) as a function of α ($\alpha=[\text{succinate}]/KR$); the curves for $\bar{R}*$ and $\bar{Y}^*$ are dashed. (B) Values of ν in black corresponding to the left ordinate and values of the derivatives $d\bar{R}/d\alpha$ and $d\bar{R}*/d\alpha$ in blue corresponding to the right ordinate, with the latter as a dashed curve. While curves for $\bar{R}$ and $\bar{R}^*$ in A cross at α_{50} (defined by $(-1)/(1-\lambda c)$, with a value 0.5 (see Material and Methods, Eqn 16) at this point, the curves for $\bar{Y}$ and $\bar{Y}^*$ also cross at $\alpha=(-1)/(1-\lambda c)$, but their value is $\bar{Y}=\bar{Y}^*=[+\lambda c(\lambda-1)-1]/[2\lambda(1-c)]$, which only equals 0.5 for $\lambda=1/c$. For the conditions presented here, at the cross point: $\bar{Y}=\bar{Y}^*=0.19$. The original analysis based on the MWC model with four subunits used the values of $K_R=4.75\times10-4$ M, $L=4$ and $c=0.001$ [45]. The model was re-analyzed by generating theoretical curves with the original parameters for a tetramer and performing a least-squares fit to obtain the best parameters for the hexamer, resulting in a change of the value of c to 0.26, when K_R and L were unchanged. For ATCase, ligand depletion was not considered, since experimental results were obtained at concentrations of the enzyme for which ligand depletion was negligible and even in overproducing strains [62] ligand depletion is only a minor effect *in vivo*.
doi:10.1371/journal.pone.0008449.g005

the ratio of the derivatives of $\bar{R}$ and $\bar{R}^*$ at 50% (Figure 1) corresponds precisely to the value of $\nu_{max}=34$. The value of ν represents the intrinsic cooperativity of the protein and ν_{max} is not affected by ligand-depletion. For various signal transduction systems, the intrinsic cooperativity can, however, be modulated by ligand depletion effects. In order to characterize the effects of ligand depletion on cooperativity we calculated the effective ν_{max} by correcting ν for the ratio of the slopes of $\bar{R}$ and $\bar{R}^*$ for corresponding fractional activations. As shown for calmodulin (Figure 2B), as for any sensor protein that possesses intrinsic cooperativity, ligand depletion can dramatically reduce the effective cooperativity in a physiological context. Indeed, this effect can bring the effective cooperativity to near 0 (Figure 2B). Because of non-equivalence of the four calmodulin ligand-binding sites, the non-identical dissociation constants for the sites result in the value of $\nu_{max}\ll4$ in Figure 2B.

Discussion

Since many cellular control networks involve cooperative interactions among their components, modeling in the context of complete systems requires accurate estimations of the cooperativity of individual reactions. Since ligand depletion can exert an attenuating effect on cooperativity, it is important to have reliable estimates in the absence of ligand depletion. As illustrated in Figure 3, the Hill coefficient as applied to the state function of the MWC model, $\bar{R}$ (equivalent to a dose-response curve) clearly does not reflect the correct cooperativity of the response, due to the invariance in the shape, as visualized in the Hill plot presented in Figure 4. As a result, when applied to the classical allosteric enzyme, aspartate transcarbamylase, the difference between the functions for ligand binding ($\bar{Y}$) and change of conformational state ($\bar{R}$) are not meaningfully characterized by their respective Hill coefficients. The value of $n_H=1.24$ for ($\bar{Y}$) accurately reflects the correct degree of cooperative binding, since it contrasts with the non-cooperative case, with $n_H=1.0$. In comparison, for $\bar{R}$ the observed value of $nH=1.12$ is not meaningful, since the non-cooperative case, as expressed by the corresponding "equivalent monomer," displays a value of $n_H=0.187$. The correct extent of cooperativity of $\bar{R}$ can be calculated from the ratio of these two values, or directly from the new index, ν, as defined in Eqn 15, with $\nu=6.0$ in the case of $\bar{R}$ for ATCase.

The results presented here demonstrate that neither dynamic range nor effective cooperativity are properties of sensing proteins that can be considered to be invariant; rather than are likely to vary according to the organ, tissue, or cell-type. The concentrations of most signaling

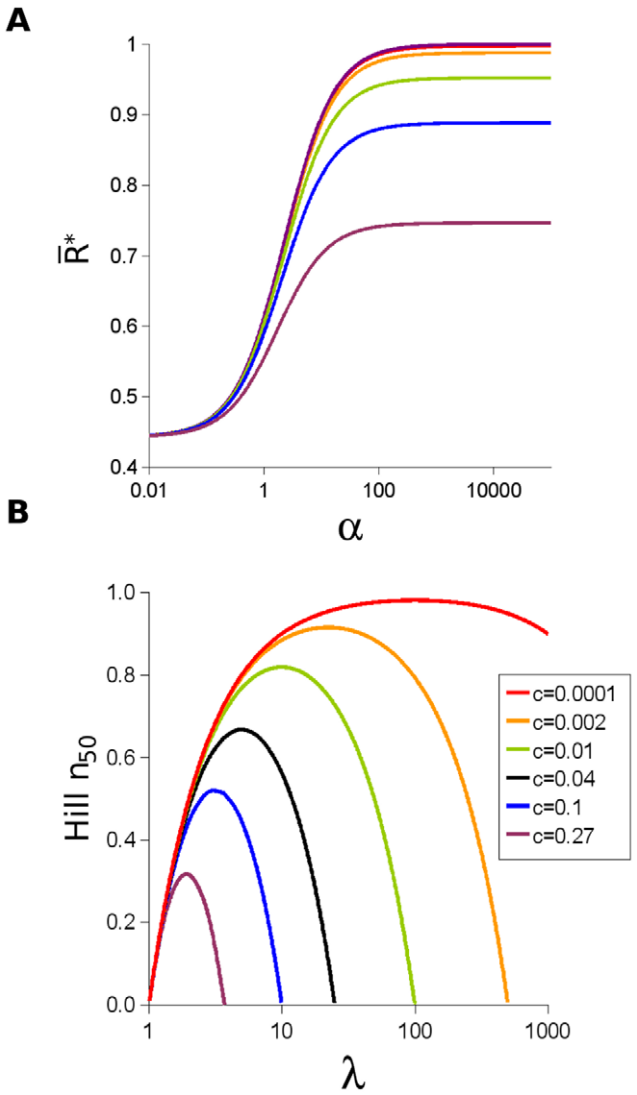

Figure 6. Properties of equivalent monomers. (A) Dependence of the state function $\bar{R}*$ versus α on the value of c. Six values of c are presented corresponding to the color code indicated in the inset to the figure. (B) Value n_50, the Hill coefficient at $\bar{R}* = 0.5$, as a function of the monomer transition parameter λ for the six values of c presented in (A) with the same color code.
doi:10.1371/journal.pone.0008449.g006

proteins are similar to their dissociation constants, in the nano- to micro-molar range, as for example in the well-characterized compartment of the PSD signaling complex of dendritic spines [50]. For calmodulin, it is particularly clear that ligand-depletion is common under physiological conditions, as shown in Figure 2, with the exact consequences depending on the tissue. Related examples include the interaction of calmodulin with other downstream components, such as calcineurin in the micromolar range [51]. While dose-response curves provide the basic characterizations of "systems" and therefore lie at the core of pharmacological treatments, in the analyses presented here we show that dose-response parameters cannot be reused directly in models of signaling systems. Instead one needs to build "mechanistic" models and run parameter-fitting approaches for particular conditions. Although we emphasized the effects of ligand depletion using the allosteric model [1], the general conclusions would apply equally well to other mechanistic descriptions, including the classical Adair-Klotz formulation [52].

It is also important to emphasize that cooperativity and dynamic range can change with the level of expression of the sensor. It is known that the available pools of signaling proteins can be quickly modified by segregation, inhibition, or change in expression. Because of the extreme cooperativity of the flagellar motor, ligand depletion dramatically increases the dynamic range of the system, as shown in Figure 1, making this system extremely sensitive to concentration effects. Since flagellar protein concentration will ultimate influence these properties, it is therefore clear that by changing the number of motors, bacterial cells could enhance their adaptation properties. Since the number of flagella per bacterial cell can vary considerably [53], this parameter must be taken into account for any complete characterization of chemotaxis [54]. More generally, the use of ligand depletion could be a widespread physiological mechanism for cells to adapt non-linear properties and sensitivity ranges to evolving environmental conditions. Because ligand depletion can decrease the effective cooperativity of transducers *in situ* and increases the dynamic range, we propose that modifying the concentration of the sensor may be a powerful way to adapt quickly to a new environment and switch from a measurement mode to a detection mode.

As modeling of biological phenomena encompasses systems of increasing complexity, particularly in efforts to develop realistic models of the nervous system [55–59], it is important to represent the underlying molecular processes as accurately as possible. The results presented here, in line with other published findings [14,15,20–23], emphasize that cooperativity and its consequences, especially dynamic range, cannot be introduced into models as fixed parameters based on Hill coefficients estimated from *in vitro* studies. Rather, each set of reaction components must be evaluated separately with respect to effects of concentration in the system examined, in order to describe accurately the functional properties that apply.

Materials and Methods

Dose-Response Relationships for an Oligomeric Protein with Two Conformational States

We consider a multisite signaling protein that can interconvert between two functionally distinct conformational states, a more active state (R) with a high affinity for ligand (X) and a less active state (T), with a low affinity for the ligand. The partition between the two states is characterized by L, the relative intrinsic stability of the two states in the absence of ligand:

$$L = \frac{[T]}{[R]} \tag{1}$$

The affinities of the R and T states for the specifically bound ligand are characterized by the intrinsic dissociation constants: K_R and K_T. For convenience, as originally proposed in the MWC model [1], the ratio of affinities is represented by c:

$$c = \frac{K_R}{K_T} \tag{2}$$

and the parameter α is defined as the normalized ligand concentration:

$$\alpha = \frac{[X]}{K_R} \tag{3}$$

Using these parameters [1], for a protein with N sites, the binding function is given by:

$$\bar{Y} = \frac{\alpha(1+\alpha)^{(N-1)} + Lc\alpha(1+c\alpha)^{(N-1)}}{(1+\alpha)^N + L(1+c\alpha)^N} \quad (4)$$

and the state function is given by:

$$\bar{R} = \frac{(1+\alpha)^N}{(1+\alpha)^N + L(1+c\alpha)^N} \quad (5)$$

In order to generalize Eqn 5 to multiple ligands, we introduce a new parameter, Ω, to describe the relative stabilization of the T state by a ligand:

$$\Omega = \frac{1+c\alpha}{1+\alpha} \quad (6)$$

For a protein with N sites, at any concentration of X, the state function $\bar{R}$ is then given with respect to Ω by:

$$\bar{R} = \frac{1}{1+L\Omega^N} \quad (7)$$

For m different ligands binding on multiple sites to the same protein, Ω^N in the above equation is replaced by the product of Ω^{N_i} for the respective ligands:

$$\bar{R} = \frac{1}{1+L\prod_{i=1}^{i=m}\Omega_i^{N_i}} \quad (8)$$

Since $\Omega^{N_i} = 1$ if the number of sites is 0, the concentration of the effector is 0, or the affinities for the R and T states are identical, this formula actually describes the absolute state function, modulated by any possible effector [43].

Calculation of Ligand Depletion

Under conditions of significant ligand depletion, i.e. ligand concentrations in the same range as dissociation constant, the degree of ligand binding to its receptor cannot be calculated directly from the total concentration, because only a fraction of this concentration is "free" and available to participate in the binding equilibrium. For any total concentration, the corresponding free concentration can be calculated with respect to a given receptor concentration as one of the roots of the appropriate second-order equation [22]. However, a simpler approach was used here. We define the parameter $\bar{R}'$ to define $\bar{R}$ as a function of the total concentration. For each value of $\bar{R}'$, the corresponding value of the total concentration, expressed as α_{total} total, is calculated from the equation:

$$\alpha_{\text{total}} = \alpha_{\text{free}} + \bar{Y}\cdot[C_S] \quad (9)$$

where $[C_S]$ is the concentration of ligand binding sites. Multiplying $\bar{Y}$ by $[C_S]$ therefore provides a correction factor that when added to α_{free} gives α_{total}.

The Index of Cooperativity, v, for an Oligomer with Respect to Its Equivalent Monomer

In order to evaluate the cooperativity of $\bar{R}$ versus α, it must be compared to the properties of a single-site "equivalent monomer." For any conditions of N, L, and Ω, we postulate an equivalent monomer with transitions between monomeric states R^* and T^* defined by:

$$\lambda = \frac{[T^*]}{[R^*]} \quad (10)$$

where

$$\lambda^N = L \quad (11)$$

For a symmetrical system composed of identical ligand-binding sites, the fraction of monomers in the R^* state is given by:

$$\bar{R}^* = \frac{1}{1+\lambda\Omega} \quad (12)$$

In this case, the curves for $\bar{R}$ and $\bar{R}^*$ as a function of α cross at $\bar{R} = \bar{R}^* = 0.5$. The slopes of $\bar{R}$ and $\bar{R}^*$ versus α are obtained from, respectively, the following derivatives:

$$\frac{d\bar{R}}{d\alpha} = \frac{NL\Omega^{(N-1)}(1-c)}{\left(1+L\Omega^N\right)^2(1+\alpha)^2} \quad (13)$$

and

$$\frac{d\bar{R}^*}{d\alpha} = \frac{\lambda(1-c)}{(1+\lambda\Omega)^2(1+\alpha)^2} \quad (14)$$

The intrinsic cooperativity or amplification of the signal reflected by the properties of $\bar{R}$ can then be obtained by a new parameter, represented by the coefficient v (the Greek letter nu) and calculated from the ratio of the two derivatives above ($v = [d\bar{R}/d\alpha]/[d\bar{R}^*/d\alpha]$) which simplifies to the equation:

$$v = \frac{N(1+\lambda\Omega)^2(\lambda\Omega)^{(N-1)}}{\left(1+(\lambda\Omega)^N\right)^2} \quad (15)$$

The coefficient v gives the cooperativity of the oligomeric protein for the state function $\bar{R}$ in a manner analogous to n_H (the Hill coefficient) for the binding function ($\bar{Y}$), which describes cooperativity with respect to a monomer that in every case displays a value of $n_H = 1$. In contrast, when applied to $\bar{R}^*$, the Hill coefficient is likely to be substantially less than 1 (see Figure 6B), demonstrating why the Hill coefficient is inappropriate for estimating the cooperativity of $\bar{R}$. For a given value of λ the lower limit of $\bar{R}^*$ is given by $1/(1+\lambda)$ and the upper limit of $\bar{R}^*$ is given by $1/(1+\lambda c)$, with the curves for $\bar{R}^*$ as a function of α described in Figure 6A. The intersection of the curves for $\bar{R}$ and $\bar{R}^*$ at 0.5 corresponds to the value of α defined as α_{50} and is given by:

$$\alpha_{50} = \frac{\lambda-1}{1-\lambda c} \quad (16)$$

Under these conditions, $\Omega = 1/\lambda$ and the $\bar{R}$ cooperativity parameter is at its maximal value: $v_{max} = N$ (whereas $v < N$ for all other values of α).

Derivation of the Hill Coefficient for an Equivalent Monomer

With respect to ligand binding, compared to Eqn 4 for fractional ligand binding, $\bar{Y}$, within the context of the two state MWC model [1], the corresponding equation for fractional binding to the equivalent monomer, $\bar{Y}^*$, is given by:

$$\bar{Y}^* = \frac{\alpha + \lambda c\alpha}{1 + \alpha + \lambda(1 + c\alpha)} \tag{17}$$

The Hill coefficient, n_H, is defined by the derivative:

$$n_H = \frac{\mathrm{d}\,\log \frac{\bar{Y}^*}{1 - \bar{Y}^*}}{\mathrm{d}\,\log \alpha} \tag{18}$$

Substituting Eqn 17 for $\bar{Y}^*$ yields:

$$n_H = \frac{\mathrm{d}\,\log \frac{\alpha + \lambda c\alpha}{1 + \lambda}}{\mathrm{d}\,\log\,\alpha} = \frac{\mathrm{d}\,\log\,\alpha}{\mathrm{d}\,\log\,\alpha} = 1 \tag{19}$$

In contrast, n_H for $\bar{R}^*$ as defined by Eqn 12 yields the derivative:

$$n_H = \frac{\mathrm{d}\,\log \frac{\bar{R}^*}{1 - \bar{R}^*}}{\mathrm{d}\,\log \alpha} \tag{20}$$

Substituting Eqn 12 for $\bar{R}^*$ yields:

$$n_H = \frac{\alpha - c\alpha}{(1 + \alpha)(1 + c\alpha)} \tag{21}$$

Therefore, since $0 < c < 1$ and $\alpha > 1$, it is clear that:

$$\frac{\alpha - c\alpha}{(1 + \alpha)(1 + c\alpha)} < \frac{\alpha}{(1 + \alpha)(1 + c\alpha)} < \frac{\alpha}{(1 + \alpha)} < 1 \tag{22}$$

and hence for $c > 0$, the Hill coefficient for $\bar{R}^*$ must be < 1 (additional details in M. Stefan, Thesis, University of Cambridge, 2009).

Acknowledgments

The authors are grateful to Philippe Cluzel and Victor Sourjik for their raw data and enlightening discussions and to Rava A. da Silveira and Nick Goldman and his group for help with the mathematics.

Author Contributions

Conceived and designed the experiments: SJE MIS NLN. Performed the experiments: SJE MIS NLN. Analyzed the data: SJE MIS NLN. Wrote the paper: SJE MIS NLN.

References

1. Monod J, Wyman J, Changeux JP (1965) On the nature of allosteric transitions: A plausible model. J Mol Biol 12: 88–118.
2. Bray D, Duke T (2004) Conformational spread: the propagation of allosteric states in large multiprotein complexes. Annu Rev Biophys Biomol Struct 33: 53–73.
3. Changeux JP, Edelstein SJ (2005) Allosteric mechanisms of signal transduction. Science 308: 1424–8.
4. Hill A (1910) The possible effects of the aggregation of the molecules of haemoglobin on its dissociation curves. J Physiol 40: 4–7.
5. Edelstein S (1975) Cooperative interactions of hemoglobin. Annu Rev Biochem 44: 209–232.
6. Ferdinand W (1966) The interpretation of non-hyperbolic rate curves for two-substrate enzymes. a possible mechanism for phosphofructokinase. Biochem J 98: 278–83.
7. Whitehead EP (1978) Co-operativity and the methods of plotting binding and steady-state kinetic data. Biochem J 171: 501–4.
8. Weiss JN (1997) The hill equation revisited: uses and misuses. Faseb J 11: 835–41.
9. Qian H (2008) Cooperativity and specificity in enzyme kinetics: a single-molecule time-based perspective. Biophys J 95: 10–7.
10. Kamata K, Mitsuya M, Nishimura T, Eiki J, Nagata Y (2004) Structural basis for allosteric regulation of the monomeric allosteric enzyme human glucokinase. Structure 12: 429–38.
11. Kim YB, Kalinowski SS, Marcinkeviciene J (2007) A pre-steady state analysis of ligand binding to human glucokinase: evidence for a preexisting equilibrium. Biochemistry 46: 1423–31.
12. Goldbeter A, Koshland JDE (1981) An amplified sensitivity arising from covalent modification in biological systems. Proc Natl Acad Sci U S A 78: 6840–4.
13. Kim SY, Ferrell JJE (2007) Substrate competition as a source of ultrasensitivity in the inactivation of Wee1. Cell 128: 1133–45.
14. Buchler NE, Louis M (2008) Molecular titration and ultrasensitivity in regulatory networks. J Mol Biol 384: 1106–19.
15. Bluthgen N, Bruggeman FJ, Legewie S, Herzel H, Westerhoff HV, et al. (2006) Effects of sequestration on signal transduction cascades. FEBS J 273: 895–906.
16. Koshland JDE (1996) The structural basis of negative cooperativity: receptors and enzymes. Curr Opin Struct Biol 6: 757–61.
17. Kister J, Poyart C, Edelstein S (1987) An expanded two-state allosteric model for interactions of human hemoglobin A with nonsaturating concentrations of 2,3-diphosphoglycerate. J Biol Chem 262: 12085–12091.
18. Rao CV, Glekas GD, Ordal GW (2008) The three adaptation systems of bacillus subtilis chemotaxis. Trends Microbiol 16: 480–7.
19. Hansen CH, Endres RG, Wingreen NS (2008) Chemotaxis in Escherichia coli: a molecular model for robust precise adaptation. PLoS Comput Biol 4: e1.
20. Goldstein A, Barrett RW (1987) Ligand dissociation constants from competition binding assays: errors associated with ligand depletion. Mol Pharmacol 31: 603–9.
21. Swillens S (1995) Interpretation of binding curves obtained with high receptor concentrations: practical aid for computer analysis. Mol Pharmacol 47: 1197–203.
22. Martinez K, Corringer P, Edelstein S, Changeux JP, Merola F (2000) Structural differences in the two agonist binding sites of the torpedo nicotinic acetylcholine receptor revealed by time-resolved fluorescence spectroscopy. Biochemistry 39: 6979–90.
23. Legewie S, Bluthgen N, Herzel H (2005) Quantitative analysis of ultrasensitive responses. FEBS J 272: 4071–9.
24. Kentner D, Sourjik V (2006) Spatial organization of the bacterial chemotaxis system. Curr Opin Microbiol 9: 619–24.
25. Belas R, Zhulin IB, Yang Z (2008) Bacterial signaling and motility: sure bets. J Bacteriol 190: 1849–56.
26. Xia Z, Storm DR (2005) The role of calmodulin as a signal integrator for synaptic plasticity. Nat Rev Neurosci 6: 267–76.
27. Gsponer J, Christodoulou J, Cavalli A, Bui JM, Richter B, et al. (2008) A coupled equilibrium shift mechanism in calmodulin-mediated signal transduction. Structure 16: 736–46.
28. Schachman H (1988) Can a simple model account for the allosteric transition of aspartate transcarbamoylase? J Biol Chem 263: 18583–18586.
29. Lipscomb W (1994) Aspartate transcarbamylase from Escherichia coli: activity and regulation. Adv Enzymol Relat Areas Mol Biol 68: 67–151.
30. Cluzel P, Surette M, Leibler S (2000) An ultrasensitive bacterial motor revealed by monitoring signaling proteins in single cells. Science 287: 1652–5.
31. Sourjik V, Berg HC (2002) Binding of the Escherichia coli response regulator CheY to its target measured in vivo by fluorescence resonance energy transfer. Proc Natl Acad Sci U S A 99: 12669–74.
32. Thomas DR, Morgan DG, DeRosier DJ (1999) Rotational symmetry of the C ring and a mechanism for the flagellar rotary motor. Proc Natl Acad Sci U S A 96: 10134–9.
33. McEvoy MM, Bren A, Eisenbach M, Dahlquist FW (1999) Identification of the binding interfaces on CheY for two of its targets, the phosphatase CheZ and the flagellar switch protein fliM. J Mol Biol 289: 1423–33.

34. Duke TA, Le Novère N, Bray D (2001) Conformational spread in a ring of proteins: a stochastic approach to allostery. J Mol Biol 308: 541–53.
35. Alon U, Camarena L, Surette MG, Aguera y Arcas B, Liu Y, et al. (1998) Response regulator output in bacterial chemotaxis. EMBO J 17: 4238–48.
36. Scharf BE, Fahrner KA, Turner L, Berg HC (1998) Control of direction of flagellar rotation in bacterial chemotaxis. Proc Natl Acad Sci U S A 95: 201–6.
37. Clapham DE (2007) Calcium signaling. Cell 131: 1047–58.
38. Stefan MI, Edelstein SJ, Le Novère N (2008) An allosteric model of calmodulin explains differential activation of PP2B and CaMKII. Proc Natl Acad Sci U S A 105: 10768–73.
39. Porumb T (1994) Determination of calcium-binding constants by flow dialysis. Anal Biochem 220: 227–37.
40. Kakiuchi S, Yasuda S, Yamazaki R, Teshima Y, Kanda K, et al. (1982) Quantitative determinations of calmodulin in the supernatant and particulate fractions of mammalian tissues. J Biochem 92: 1041–8.
41. Karlin A (1967) On the application of "a plausible model" of allosteric proteins to the receptor of acetylcholine. J Theor Biol 16: 306–320.
42. Gerhart J, Pardee A (1962) The enzymology of control by feedback inhibition. J Biol Chem 237: 891–896.
43. Rubin M, Changeux JP (1966) On the nature of allosteric transitions: Implications of non-exclusive ligand binding. J Mol Biol 21: 265–274.
44. Gerhart J, Schachman H (1968) Allosteric interactions in aspartate transcarbamylase. II. evidence for different conformational states of the protein in the presence and absence of specific ligands. Biochemistry 7: 538–552.
45. Changeux JP, Rubin M (1968) Allosteric interactions in aspartate transcarbamylase. III. interpretations of experimental data in terms of the model of monod, wyman, and changeux. Biochemistry 7: 553–561.
46. Weber K (1968) New structural model of E. coli aspartate transcarbamylase and the amino-acid sequence of the regulatory polypeptide chain. Nature 218: 1116–9.
47. Wiley D, Lipscomb W (1968) Crystallographic determination of symmetry of aspartate transcarbamylase. Nature 218: 1119–1121.
48. Kantrowitz ER, Lipscomb WN (1990) Escherichia coli aspartate transcarbamoylase: the molecular basis for a concerted allosteric transition. Trends Biochem Sci 15: 53–9.
49. Fetler L, Kantrowitz ER, Vachette P (2007) Direct observation in solution of a preexisting structural equilibrium for a mutant of the allosteric aspartate transcarbamoylase. Proc Natl Acad Sci U S A 104: 495–500.
50. Cheng D, Hoogenraad CC, Rush J, Ramm E, Schlager MA, et al. (2006) Relative and absolute quantification of postsynaptic density proteome isolated from rat forebrain and cerebellum. Mol Cell Proteomics 5: 1158–70.
51. Goto S, Matsukado Y, Mihara Y, Inoue N, Miyamoto E (1986) The distribution of calcineurin in rat brain by light and electron microscopic immunohistochemistry and enzyme-immunoassay. Brain Res 397: 161–72.
52. Stefan MI, Edelstein SJ, Le Novère N (2009) Computing phenomenologic Adair-Klotz constants from microscopic MWC parameters. BMC Syst Biol 3: 68.
53. Salvetti S, Ghelardi E, Celandroni F, Ceragioli M, Giannessi F, et al. (2007) FlhF, a signal recognition particle-like GTPase, is involved in the regulation of flagellar arrangement, motility behaviour and protein secretion in Bacillus cereus. Microbiology 153: 2541–52.
54. Endres RG, Oleksiuk O, Hansen CH, Meir Y, Sourjik V, et al. (2008) Variable sizes of Escherichia coli chemoreceptor signaling teams. Mol Syst Biol 4: 211.
55. Markram H (2006) The blue brain project. Nat Rev Neurosci 7: 153–60.
56. Le Novere N (2007) The long journey to a systems biology of neuronal function. BMC Syst Biol 1: 28.
57. Izhikevich EM, Edelman GM (2008) Large-scale model of mammalian thalamocortical systems. Proc Natl Acad Sci U S A 105: 3593–8.
58. Giegling I, Hartmann AM, Genius J, Benninghoff J, Moller HJ, et al. (2008) Systems biology and complex neurobehavioral traits. Pharmacopsychiatry 41 Suppl 1: S32–6.
59. Villoslada P, Steinman L, Baranzini SE (2009) Systems biology and its application to the understanding of neurological diseases. Ann Neurol 65: 124–39.
60. Gamble E, Koch C (1987) The dynamics of free calcium in dendritic spines in response to repetitive synaptic input. Science 236: 1311–5.
61. Henkin RI (1997) The concentration of calmodulin present in parotid cells. J Dent Res 76: 1430.
62. Gerhart JC, Holoubek H (1967) The purification of aspartate transcarbamylase of Escherichia coli and separation of its protein subunits. J Biol Chem 242: 2886–92.